Minimal Elastographic Modeling of Breast Cancer for Model Based Tumor Detection in a Digital Image Elasto Tomography (DIET) System

Thomas F Lotz[a], Natalie Muller[a], Christopher E. Hann[b], J. Geoffrey Chase[a]

[a] Centre for Bioengineering, Dept of Mechanical Engineering
[b] Dept of Electrical and Computer Engineering
University of Canterbury, Christchurch, NZ

ABSTRACT

Digital Image Elasto Tomography (DIET) is a non-invasive breast cancer screening technology that images the surface motion of a breast under harmonic mechanical actuation. A new approach capturing the dynamics and characteristics of tumor behavior is presented. A simple mechanical model of the breast is used to identify a transfer function relating the input harmonic actuation to the output surface displacements using imaging data of a silicone phantom. Areas of higher stiffness cause significant changes of damping and resonant frequencies as seen in the resulting Bode plots. A case study on a healthy and tumor silicone breast phantom shows the potential for this model-based method to clearly distinguish cancerous and healthy tissue as well as correctly predicting the tumor position.

Keywords - Breast cancer, Mechanical breast model, Transfer function, Digital Image Elasto Tomography, Elastography.

1. INTRODUCTION

Breast cancer is one of the most common types of cancer in women worldwide[1]. X-ray Mammography is currently the only approved large scale breast screening modality. However, due to the radiation exposure and breast compressions, mammography screening programmes have resulted in poor compliance rates[2]. Furthermore, breast screening programs are often not available in developing countries due to the relatively high costs involved[3] and the mostly rural populations with limited access to specialised radiology clinics[4].

Digital Image Elasto Tomography (DIET) is an elastographic imaging technology for non-invasive and low cost breast cancer screening[5]. DIET aims to generate a three dimensional representation of elastic properties throughout the breast volume, based on the high stiffness contrast differences of 300% to 1500% between cancerous and healthy tissue in the breast[6]. The technology is highly portable and does not required specialized operator skills, making it well suitable for remote screening applications at a low cost. Proof of concept testing has been performed on silicone phantom breasts[7] and in vivo trials are underway with good initial results.

Mechanical vibrations are introduced into the breast and the resulting surface oscillations are captured by digital cameras surrounding the breast, tracking fiducial markers on the breast's surface[5,8]. The oscillating surface motion is analyzed to detect disturbances in observed vibration patterns, which indicate a stiffer inclusion within the tissue. Finite Element[5] (FEM) or surface based methods[7] can be used to provide an estimate of the inclusion's location and size. While FEM can provide full 3D elastography data, the inverse solutions involved are typically computationally expensive[9] and the linear stress-strain assumptions will not necessarily always hold. A simpler analysis approach that could be performed in real-time is desired to provide immediate diagnostic information after imaging.

Due to the distinct vibration response of every point on the breast's surface, diagnostic information could be enhanced by analyzing the full frequency response of the surface. This research proposes a diagnostic metric based on the frequency response of the oscillating breast surface. A minimal modeling concept is introduced to capture the essential dynamics of breast responses that characterize tumor behavior. A simple spring-mass-damper model is used to model the response at each point on the surface. By identifying the transfer functions of these responses, elastic model parameters can be used

to locate a stiffer inclusion. This study thus presents a model-based diagnostic analysis approach, which is veryfied in a case study in vitro on two silicone phantom breasts.

2. METHODOLOGY

2.1 Experimental setup and data acquisition

The experimental setup and silicone phantoms shown in Figure 1 are used to obtain imaging data. A vibration actuator induces oscillating sinusoidal vibrations into the phantom and five cameras surrounding the breast capture its surface motion by synchronized imaging with a strobe system[10]. Breast surface motion is tracked and parameterized to provide a displacement and phase map for the entire surface in 3D. Two silicone phantom breasts of equal geometry and healthy tissue properties (E=3kPa) are used. The cancerous phantom has a tumor of 20mm diameter with a stiffness contrast of 10x.

Figure 1: A silicone phantom with fiducial markers (left); The experimental setup with the vibration actuator in the middle, and five cameras with strobe lights surrounding it.

A rectangle polar coordinate system is used, with α defining the elevation and θ defining the rotational angle, as shown in Figure 3. The surface is discretized into intervals of α and θ and the mean value of all tracked markers is used for each interval to account for uneven marker coverage. With imaging sets taken at a range of frequencies covering at least the first resonant frequency, Bode plots can be plotted for each α and θ segment on the breast surface. Bode plots for a healthy and cancerous silicone phantom at the tumor's position at $\alpha = 25°$ and $\theta = 180°$, and at $\alpha = 25°$ and $\theta = 25°$, respectively, are shown in Figure 2. Frequency steps were chosen between 8-50Hz, with a resolution of 2Hz.

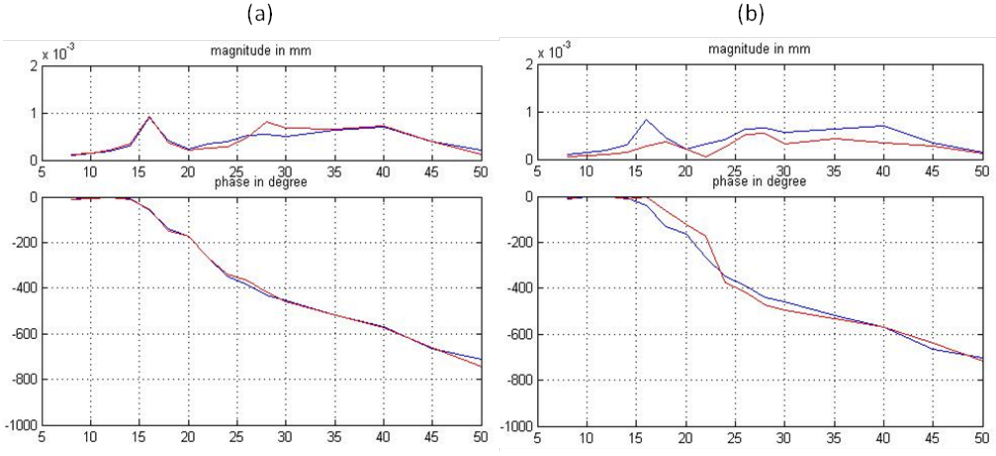

Figure 2: Example of Bode plots obtained on the surface of the breast, at two different locations, (a) $\alpha = 25°$, $\theta = 25°$; (b) $\alpha = 25°$, $\theta = 180°$ (tumor position). Blue: healthy phantom data; Red: tumor phantom data.

Clear differences between the healthy and tumor responses at the tumor's position are evident, seen in the differences evident around the first peak at 16 Hz shown in Figure 2(b). The first healthy resonant frequency lies at about 16 Hz, whereas the first resonant frequency at the tumor's position is shifted to about 18 Hz. Since all this information is contained in the region surrounding the first resonant peak, for simplicity, only frequencies up to 20 Hz are considered in the modeling.

2.2 Mechanical breast model

A simplified sketch of the breast is presented in Figure 3 (a). The data of the motion captured by the camera system is dependent on the surface location (α and θ). The breast response is modeled by a a single spring-mass-damper system, shown in Figure 3 (b). The input $u(t)$ is the excitation of the breast by the actuator. The mass m is modeled as a function of α and θ to account for the distance to the actuation source. The stiffness k and damping b of the breast vary depending on both α and θ. Near a tumor the stiffness $k(\alpha,\theta)$ and damping $b(\alpha,\theta)$ are expected to increase due to the stiffer elastic properties of cancerous tissue. For a healthy breast $b(\alpha,\theta)$ and $k(\alpha,\theta)$ are expected to be constant throughout the whole breast.

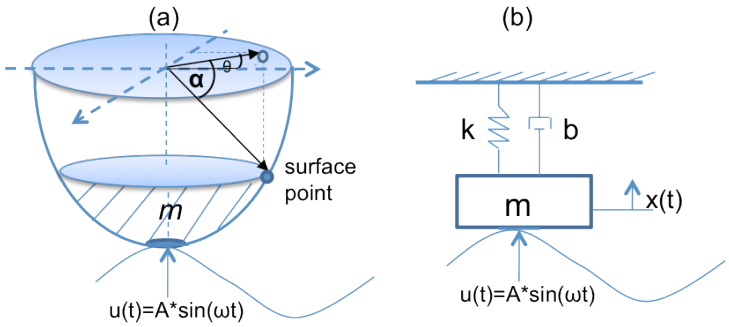

Figure 3: (a) Schematic of the breast; (b) Mechanical model of the breast

The resulting equation of the single spring-mass-damper model in Figure 3(b) is defined:

$$m(\alpha,\theta)\ddot{x}(t) + b(\alpha,\theta)\dot{x}(t) + k(\alpha,\theta)x(t) = u(t) \tag{1}$$

where:

$$u(t) = A\sin(\omega t) \tag{2}$$

and ω is the excitation frequency. Equation (1) is rewritten in the form:

$$\ddot{x}(t) + \bar{b}(\alpha,\theta)\dot{x}(t) + \bar{k}(\alpha,\theta)x(t) = k_0 u(t) \tag{3}$$

where:

$$\bar{b}(\alpha,\theta) = \frac{b(\alpha,\theta)}{m(\alpha,\theta)} \quad ; \quad \bar{k}(\alpha,\theta) = \frac{k(\alpha,\theta)}{m(\alpha,\theta)} \quad ; \quad k_0(\alpha,\theta) = \frac{1}{m(\alpha,\theta)} \tag{4}$$

Equation (3) is then rewritten as:

$$\ddot{x}(t) + 2\xi(\alpha,\theta)\omega_n(\alpha,\theta)\dot{x}(t) + \omega_n^2(\alpha,\theta)x(t) = k_0(\alpha,\theta)u(t) \tag{5}$$

where ω_n is the natural frequency and ξ is the damping ratio of the breast defined by:

$$\omega_n(\alpha,\theta) = \sqrt{\frac{k(\alpha,\theta)}{m(\alpha,\theta)}} \quad ; \quad \xi(\alpha,\theta) = \frac{b(\alpha,\theta)}{2\sqrt{k(\alpha,\theta)m(\alpha,\theta)}} \tag{6}$$

Taking the Laplace transform of Equation (5) yields:

$$\left(s^2 + 2\xi(\alpha,\theta)\omega_n(\alpha,\theta)s + \omega_n^2(\alpha,\theta)\right)X(s) = k_0(\alpha,\theta)U(s) \tag{7}$$

The transfer function is thus defined:

$$s^2 + G_{\alpha,\theta}(s) = \frac{X}{U} = \frac{k_0(\alpha,\theta)}{s^2 + 2\xi(\alpha,\theta)\omega_n(\alpha,\theta)s + \omega_n^2(\alpha,\theta)} \tag{8}$$

The frequency transfer function is obtained from Equation (8) by setting $s=j\omega$:

$$G_{\alpha,\theta}(j\omega) = \frac{k_0(\alpha,\theta)}{(\omega_n{}^2(\alpha,\theta) - \omega^2) + 2\xi(\alpha,\theta)\omega_n(\alpha,\theta)j\omega} \tag{9}$$

where ω is the excitation frequency.

The displacement of the surface motion in dB is:

$$\left|G_{\alpha,\theta}(j\omega)\right|_{\text{model}} = 20\log_{10}\left(\left|\frac{k_0(\alpha,\theta)}{(\omega_n{}^2(\alpha,\theta) - \omega^2) + 2\xi(\alpha,\theta)\omega_n(\alpha,\theta)j\omega}\right|\right) \tag{10}$$

And the phase in degrees:

$$\varphi\left(G_{\alpha,\theta}(j\omega)\right)_{\text{model}} = \arctan\left(\frac{RE(G_{\alpha,\theta}(j\omega))}{IM(G_{\alpha,\theta}(j\omega))}\right)\frac{180}{\pi} \tag{11}$$

2.2 Parameter identification and normalization

Damping $\xi(\alpha,\theta)$ and natural frequency $\omega_n(\alpha,\theta)$ are estimated for each surface segmet with nonlinear least squares.

For a healthy breast it is assumed that damping is constant for a given α, as θ varies from 0 to 2π, whereas damping is expected to be different at the location of a tumor θ. The natural frequency would behave similarly. Thus, to normalize the effect of α, measures of relative change in damping ξ and natural frequency ω_n are defined:

$$\xi_{norm}(\alpha,\theta) = \frac{\hat{\xi}(\alpha,\theta)}{\min_\alpha(\hat{\xi}(\alpha))} \quad ; \quad \omega_{n\,norm}(\alpha,\theta) = \frac{\hat{\omega}_n(\alpha,\theta)}{\min_\alpha(\hat{\omega}_n(\alpha))} \tag{12}$$

3. RESULTS

Model fits to the Bode plots at $\alpha = 25°$ and $\theta = 180°$ for the healthy and cancerous case are shown in Figure 4. The mean error value for displacement over θ for the healthy case is 0.56 dB, with a 90th percentile of 1.18 dB. These values are relatively small compared to the absolute change in displacement which is about 20 dB as seen in Figure 4. There is also a good match of the phase, with absolute mean errors of 6.0° and a 90th percentile of 12.5°.

For the healthy case, the mass is a function of α only and in both cases the mass increases as a function of α. This result matches the mass representation of Figure 3 (a). For the cancer case there is a noticeable increase in mass near $\theta = 180°$, which corresponds to the tumor location. This result is expected since a tumor would add to the effective mass seen at a surface point close to it.

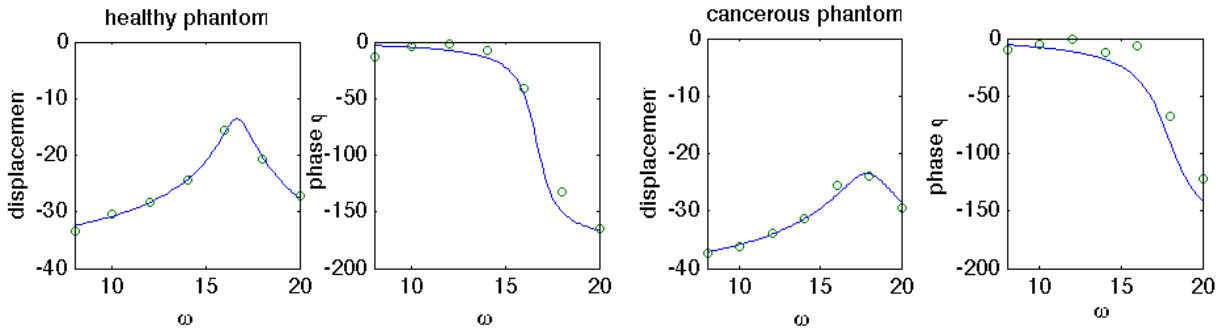

Figure 4: Model fits to the Bode plots at $\alpha = 25°$ and $\theta = 180°$ for the healthy (left) and cancerous case (right) (model ≡ '-'; data ≡ 'o')

Figure 5 shows the results obtained for normalized damping $\xi_{norm}(\alpha,\theta)$ and natural frequency $\omega_{n,norm}(\alpha,\theta)$. Both metrics hardly change in the healthy case shown in Figure 5 (top), but there are significant changes in the cancerous phantom at the location of the tumor, as shown in Figure 5 (bottom). The position of the tumor is predicted to be at an angle of θ=180° and α=30°.

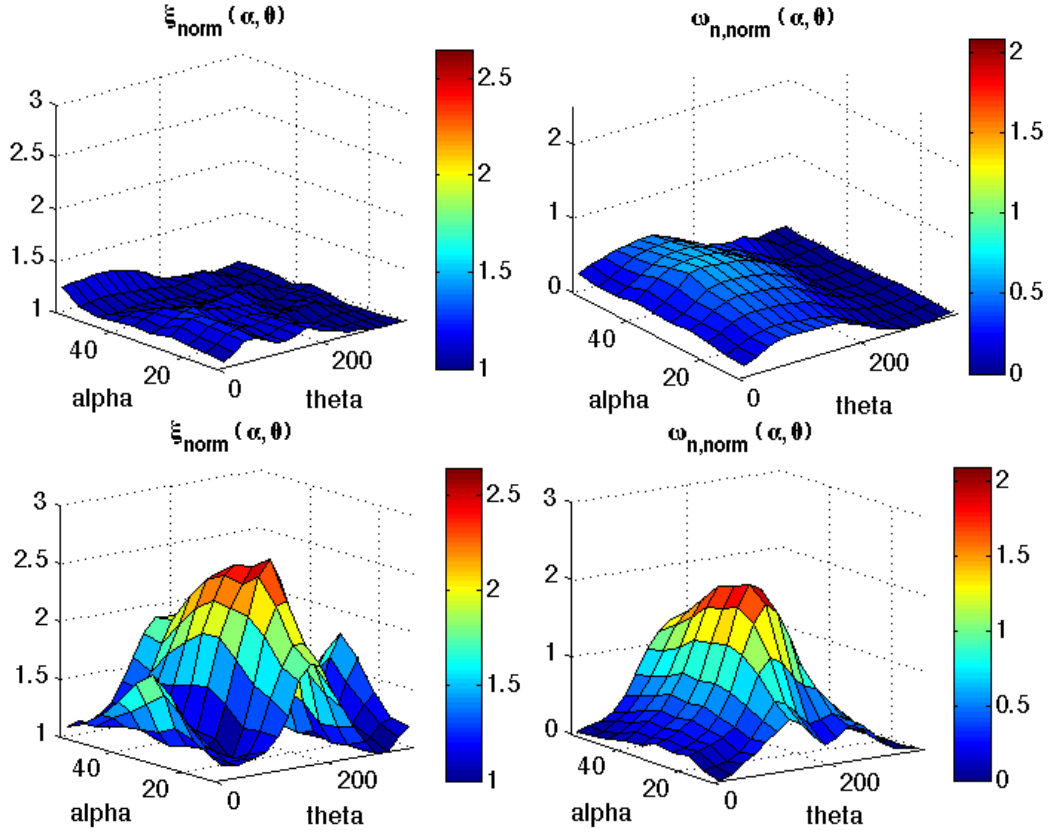

Figure 5: Surface plot for $\xi_{norm}(\alpha,\theta)$and $\omega_{n,norm}(\alpha,\theta)$; (top) healthy case; (bottom) tumor case

4. DISCUSSION AND CONCLUSIONS

The proposed minimal modeling approach is able to capture frequency response data from the surface of an oscillating breast phantom. Due to the simplicity of the model, only data up to the first resonant peak is required. Model fits were very good, in both the healthy and the cancerous phantom on all surface segments. Normalization with regard to α and θ managed to capture relative changes of damping and natural frequency around the breast, so that in principle, differences in breast size or shape are effectively removed, allowing for a robust, repeatable method.

Normalized damping $\xi_{norm}(\alpha,\theta)$ and natural frequency $\omega_{n,norm}(\alpha,\theta)$ values identified over the surface of the breast show a distinctive difference around the location of the tumor. In particular θ matches the position of the tumor exactly. This result can be expected due to the concentric source of actuation with regards to θ. The identified value for α differs from the angle of the tumor inclusion, which is due to the asymmetrical geometry of the breast relative to the vibration source.

A potential limitation of the proposed method is the oversimplified mechanical model of the breast. In our own experiments on phantoms and in-vivo, we have observed at least a second resonant peak in most cases, which can only be captured by more complex modeling approaches. While the diagnostic performance could possibly be improved with better modeling, the simple approach presented here already shows robust and good results in this silicone phantom data. More thorough validation of this method in-vitro and in-vivo will be required to assess its performance regarding tumor size and depth, and on varying physiological breast shapes. Full validation was not the intention of this initial study and is left for future investigation.

A simple modeling approach has been presented to match elastic breast behavior. By imaging the frequency response of the surface of a breast, the proposed method could provide elastographic information of the breast in real time, which could indicate the presence of a tumor. Combined with a non-invasive optical imaging system, such as DIET, this approach could provide a simple screening adjunct modality to mammography.

REFERENCES

[1] S. S. Coughlin and D. U. Ekwueme, "Breast cancer as a global health concern," *Cancer epidemiology,* vol. 33, pp. 315-8, Nov 2009.

[2] M. Kriege*, et al.*, "Efficacy of MRI and mammography for breast-cancer screening in women with a familial or genetic predisposition," *The New England journal of medicine,* vol. 351, pp. 427-37, Jul 29 2004.

[3] A. Sarvazyan*, et al.*, "Cost-Effective Screening for Breast Cancer Worldwide: Current State and Future Directions," *Breast cancer,* vol. 1, pp. 91-99, Jul 2 2008.

[4] L. Yang*, et al.*, "Estimates of cancer incidence in China for 2000 and projections for 2005," *Cancer epidemiology, biomarkers & prevention,* vol. 14, pp. 243-50, Jan 2005.

[5] A. Peters*, et al.*, "Estimating elasticity in heterogeneous phantoms using Digital Image Elasto-Tomography," *Medical and biological engineering and computing,* vol. 47, pp. 67-76, Jan 2009.

[6] A. Samani*, et al.*, "Elastic moduli of normal and pathological human breast tissues: an inversion-technique-based investigation of 169 samples," *Physics in medicine and biology,* vol. 52, pp. 1565-76, Mar 21 2007.

[7] T. Lotz*, et al.*, "In vitro evaluation of surface based non-invasive breast cancer screening with Digital Image based Elasto Tomography (DIET)," in *IEEE EMBS*, Buenos Aires, 2010, pp. 3077-80.

[8] R. G. Brown*, et al.*, "Discrete Colour-based Euclidean-Invariant Signatures for Feature Tracking in a DIET Breast Cancer Screening System," presented at the SPIE Medical Imaging, San Diego, USA, 2007.

[9] A. Peters*, et al.*, "Digital image elasto-tomography: combinatorial and hybrid optimization algorithms for shape-based elastic property reconstruction," *IEEE transactions on bio-medical engineering,* vol. 55, pp. 2575-83, Nov 2008.

[10] C. E. Hann*, et al.*, "Strobe Imaging System for Digital Image-based Elasto-Tomography Breast Cancer Screening," *IEEE Transactions on Industrial Electronics,* vol. 56, pp. 3195-3202, 05 June 2009 2009.